Zonal flow production in the L-H transition in Alcator C-Mod

I Cziegler[1], G R Tynan[1], P H Diamond[1], A E Hubbard[2], J W Hughes[2], J Irby[2], J L Terry[2]

E-mail: iczieglerucsd.edu
[1] University of California San Diego, Center for Momentum Transport and Flow Organization, 9500 Gilman Drive, La Jolla, CA, 92093
[2] Massachusetts Institute of Technology, Plasma Science and Fusion Center, 175 Albany Street, Cambridge, MA, 02139

Abstract. Transitions of tokamak confinement regimes from low- to high-confinement are studied on Alcator C-Mod [1] tokamak using gas-puff-imaging (GPI) with a focus on the interaction between the edge drift-turbulence and the local shear flow. Results show that the nonlinear turbulent kinetic energy transfer rate into the shear flow becomes comparable to the estimated value of the drift turbulence growth rate at the time the turbulent kinetic energy starts to drop, leading to a net energy transfer that is comparable to the observed turbulence losses. A corresponding growth is observed in the shear flow kinetic energy. The above behavior is demonstrated across a series of experiments. Thus both the drive of the edge zonal flow and the initial reduction of turbulence fluctuation power are shown to be consistent with a lossless kinetic energy conversion mechanism, which consequently mediates the transition into H-mode. The edge pressure gradient is then observed to build on a slower (1ms) timescale, locking in the H-mode state. These results unambiguously establish the time sequence of the transition as: *first* the peaking of the normalized Reynolds power, *then* the collapse of the turbulence, and *finally* the rise of the diamagnetic electric field shear as the L-H transition occurs.

PACS numbers: 52.25.Fi, 52.35.Kt, 52.35.Mw, 52.35.Ra, 52.55.Fa, 52.70.Kz

Submitted to: *Nuclear Fusion*

1. Introduction

The transition between the low- and the high-confinement plasma states [2], or L-H transition, in tokamak devices is one of the outstanding challenges of theoretical and experimental understanding of magnetically confined fusion. As future fusion devices expect to explore operating conditions often far outside the realm of current experiments, a physics based, quantitative understanding of the L-H transition with predictive power is of critical importance. Regardless of whether the H-mode is to be achieved or avoided, the model to guide operations must connect the microscopic dynamics to the macroscopic phenomenology of plasma transport behavior. Thus achieving an understanding of the underlying microscopic physics that leads to the L-H transition is of fundamental importance in magnetic fusion research.

H-mode plasmas are characterized by a turbulence level reduced relative to low confinement regimes and strong radial electric field (E_r) shear,[3, 4] which is dominated by the ion pressure gradient in the radial force balance. Detailed studies indicate that the ion pressure gradient develops as a consequence of the L-H transition.[5] Azimuthally symmetric, turbulence-generated shear flows, usually termed "zonal flows" (ZF)[6] also appear to be associated with the LH transition[7, 8, 9]. The trigger of the transition, however, has not yet been comprehensively explained. Recent studies of the edge plasma using Langmuir probes have provided evidence that the immediate trigger of the transition is the nonlinear exchange of kinetic energy between small scale turbulence and edge zonal flows.[10, 11] Due to the potential difficulties which arise in interpreting probe signals in an environment of fluctuating plasma temperature, it is very important to ascertain the validity of these measurements via independent diagnostics.

This paper presents the first gas-puff-imaging based study of the nonlinear interaction between the small scale edge turbulence and zonal flows in a time resolved sense in typical fast L-H transitions in Alcator C-Mod. In addition to corroborating the recent findings of probe studies, detailed quantitative comparisons are presented here for the first time: the observed reduction in turbulence power is shown to be consistent with the independently measured nonlinear kinetic energy transfer rate, while the turbulent drive of the edge zonal flows caused by this exchange, taken together with experimentally determined flow damping rates, is demonstrated to be sufficient to explain the local flow generation. Comparative measurements are demonstrated on a large ensemble of plasma experiments with a radial resolution that is afforded by the use of imaging instead of Langmuir probes. Finally, we also show for the first time that the large, H-mode-like edge plasma gradient develops *after* the transient zonal flow generation and turbulence suppression phenomena, thus clearly demonstrating the temporal sequence of events that lead to the formation of the H-mode confinement regime.

2. Model equations

The spectral transfer of fluctuation power is commonly studied in a time averaged sense using cross-bispectral techniques.[12, 13, 14, 15, 16] The inherently nonstationary nature of the L-H transition, however, renders the use of such methods impossible. Thus the study of this important transition requires the treatment of the simultaneous evolution of turbulent scales and sheared $\mathbf{E} \times \mathbf{B}$ flows. The following section provides a simplified model which will motivate the choice of the specific time-resolved measures of the transfer process.

First we consider compressibility effects to be negligible on the scale of the studied evolution in the edge, and further separate our the dynamics in the direction parallel and perpendicular to the magnetic field, such that no parallel gradients are considered. Wherever compared with radial gradients, poloidal gradients are also neglected. In our preliminary analysis of the data, $\partial_\theta \langle \tilde{v}_\theta^2 \rangle$ from measurement pairs was found to be at most 1/4 of $\partial_r \langle \tilde{v}_r \tilde{v}_\theta \rangle$, and showed no significant excursions at the time of the transition. The poloidal gradient term therefore does not significantly contribute to the transfer or the transport of kinetic energy, and it is even further reduced due to the poloidal averaging employed in the paper, as it is indeed expected to vanish completely if such averaging is not limited by the GPI field of view. Then the momentum equation takes the form

$$\partial_t v_\theta + v_r \partial_r v_\theta = \mu \partial_r^2 v_\theta, \tag{1}$$

in which we use a Reynolds decomposition, $v = \langle v \rangle + \tilde{v}$, $\langle \tilde{v} \rangle = 0$, to get

$$\partial_t \langle v_\theta \rangle + \partial_r \langle \tilde{v}_r \tilde{v}_\theta \rangle = \mu \partial_r^2 \langle v_\theta \rangle. \tag{2}$$

It is assumed here that the above decomposition is a meaningful separation of times scales, such that the energy transfer process under consideration is between the complex system of fast broadband fluctuations and a much more slowly evolving flow. The mean in the definition of the Reynolds stress can be determined by either time averaging or spatial averaging. For the case of poloidal velocities, time averaging yields the slow component of the velocity spectrum, while the poloidal average provides the zonal structure of flows. Since the focus of this paper is the evolution of the slowly evolving zonal flows, $\langle . \rangle$ will therefore represent *both* a time averaging and a poloidal average of the available spatio-temporal data. Now in order to write the above as an equation for the kinetic energy of the large-scale slowly varying flow, we multiply by $\langle v_\theta \rangle$, which yields

$$\begin{aligned} \frac{1}{2} \partial_t \langle v_\theta \rangle^2 &= -\langle v_\theta \rangle \partial_r \langle \tilde{v}_r \tilde{v}_\theta \rangle + \mu \langle v_\theta \rangle \partial_r^2 \langle v_\theta \rangle \\ &= -\langle v_\theta \rangle \partial_r \langle \tilde{v}_r \tilde{v}_\theta \rangle + \frac{\mu}{2} \partial_r^2 \langle v_\theta \rangle^2 - \frac{\mu}{2} (\partial_r \langle v_\theta \rangle)^2. \end{aligned} \tag{3}$$

The first term on the RHS is often referred to as Reynolds work, the amount of work the Reynolds stress performs on the background flow in unit time. Note that (3) includes a third term on the RHS which no assumption warrants against, so we must keep it. Since $(\partial_r \langle v_\theta \rangle)^2$ is positive definite, this simple viscosity term introduces dissipation wherever there is a velocity shear, while the second term is a proper diffusion of kinetic energy.

The turbulent counterpart of this can then be obtained as the difference between (3) and the analogous equation for the total kinetic energy $(\langle v_\theta\rangle + \tilde{v}_\theta)^2 + \tilde{v}_r^2$:

$$\frac{1}{2}\partial_t\langle\tilde{v}_\perp^2\rangle = -\langle\tilde{v}_r\tilde{v}_\theta\rangle\partial_r\langle v_\theta\rangle - \frac{1}{2}\partial_r\langle\tilde{v}_r\tilde{v}_\theta^2\rangle + \mu\langle\tilde{v}_\theta\partial_r^2\tilde{v}_\theta\rangle, \tag{4}$$

where radial gradients of the radial velocity components have been neglected as small due to incompressibility and the total turbulence kinetic energy $\langle\tilde{v}_\perp^2\rangle/2$ has been introduced.

Since parallel dynamics and the coupling between pressure and potential fluctuations was explicitly not included in this simplified fluid equation, the turbulence drive term must be inserted "manually", by including a term that allows for the growth of the turbulent energy scale by the input of energy from the free energy associated with the background time-averaged plasma gradients. This drive and the dissipative effects, which are implicit in (4), both have complicated dependencies; we represent them here as a net effective linear growth $\gamma_{\rm eff}\langle\tilde{v}_\perp^2\rangle/2$, which gives the net difference between the (linear) turbulence drive and the turbulence decorrelation on the viscous scale. The dissipative terms for the slowly evolving velocity are similarly summarized as $\nu_{\rm LF}\langle v_\theta\rangle^2/2$, with the damping rate of the low-frequency flow $\nu_{\rm LF}$, including the viscous damping, trapped–passing ion collisions, plasma–neutral interaction, compressible effects, nonlinear terms etc. With that, the model equations underlying the data analysis strategy can be put together as

$$\begin{aligned}\partial_t\tilde{K} &= \gamma_{\rm eff}\tilde{K} - P - \partial_r\tilde{T}\\ \partial_t\bar{K} &= P - \partial_r\bar{T} - \nu_{\rm LF}\bar{K}\end{aligned} \tag{5}$$

where we introduced the notations

$$\begin{aligned}P &= \langle\tilde{v}_r\tilde{v}_\theta\rangle\partial_r\langle v_\theta\rangle;\\ \tilde{K} &= \frac{1}{2}\langle\tilde{v}_\perp^2\rangle, \quad \tilde{T} = \frac{1}{2}\langle\tilde{v}_r\tilde{v}_\theta^2\rangle\\ \bar{K} &= \frac{1}{2}\langle v_\theta\rangle^2, \quad \bar{T} = \langle\tilde{v}_r\tilde{v}_\theta\rangle\langle v_\theta\rangle,\end{aligned} \tag{6}$$

similarly to the analysis presented in [10, 17, 18, 19, 20]. As in Ref. [20], we refer to P as the zonal flow production term. These equations, in essence, describe the same dynamics as the Kim–Diamond predator–prey model[18], recently shown to capture the crucial points in transitions as well as limit cycle oscillations. In particular, we note that by radial force balance, here $\langle v_\theta\rangle = \langle v_E\rangle + \langle v_{d,i}\rangle$ where $\langle v_E\rangle$ is the time- and flux-surface-averaged $\mathbf{E}\times\mathbf{B}$ drift velocity and $\langle v_{d,i}\rangle$ is the time-averaged and flux-surface-averaged ion diamagnetic drift velocity associated with the ion pressure gradient profile. The ion pressure gradient, in turn, must follow an energy conservation equation that includes heat input and dissipation, and turbulent cross-field transport as proposed by Kim et al[18]. Thus the model proposed here contains the essential physics of the predator–prey model, differing from the published predator–prey models only in the fact that the Reynolds stress flow drive terms are explicitly retained to motivate the experimental data analysis.

The analyses presented in recent literature often further reduced the above equations to a 0D local set either by neglecting $\partial_r\tilde{T}$ and/or $\partial_r\bar{T}$, or by identifying

P with the total Reynolds work in one or both of the equations above. Here it is noted that $P - \partial_r \bar{T}$ represents the Reynolds work, while the total loss of local kinetic energy from the broadband spectrum via turbulence self-organization is understood to be $P + \partial_r \tilde{T}$, where $\partial_r \tilde{T}$ is a radial flux of turbulent kinetic energy, also known as turbulence spreading. From balancing the terms on the RHS of (5), it is obvious that the condition for the onset of rapid turbulence suppression is

$$\frac{P + \partial_r \tilde{T}}{\gamma_{\text{eff}} \tilde{K}} > 1 \tag{7}$$

meaning that there is enough energy transfer into the zonal flow to overcome the turbulence drive. The dynamic variables in this condition that are constructed from fluid velocities can be measured in a suitably designed experiment, while the effective growth rate of the turbulence can be estimated based on the recovery rate of turbulence in a high- to low-confinement ("back") transition, or from (5) using data obtained in regular, time-stationary L-mode. Note that in an experiment with diagnostics which allow radially resolved measurement, no further assumption is necessary on the form of any of the terms involved with the condition.

3. Experimental setup

All the experiments reported in this paper were performed on the Alcator C-Mod tokamak[1], a compact ($R_0 = 0.68\text{m}, a \simeq 0.21\text{m}$) toroidal device with a high magnetic field (up to $B_\phi \leq 8\text{T}$, with a typical $B_\phi = 5.4\text{T}$). The H-modes studied here were produced with plasma currents of $I_p = 0.8 - 1\text{MA}$ and toroidal magnetic fields of $B_\phi = 2.8 - 5.4\text{T}$ with "favorable" $\nabla \mathbf{B} \times \mathbf{B}$ direction (i.e. towards the active X-point), in lower single null (LSN) geometries. The additional heating that is required for the formation of the temperature pedestal is provided by ion-cyclotron resonance heating (ICRH) with a maximum coupled power of 2.1MW. Ohmic L-H transitions can be achieved by ramp-down of the toroidal magnetic field while keeping the plasma current constant.

Since we are interested in the immediate trigger of the L-H transition, the study focused on the few millisecond time interval just before and after the transition marked in Figure 2 as the narrow shaded area. In order to separate our results from artifacts discharges were chosen with a transition well inside the flattop period of the plasma current and several tens of milliseconds after significant changes to the heating power. The samples demonstrating the main results in Sec. 4 are from the experiment depicted in Figure 2.

The 2D fluctuation data was acquired via gas-puff-imaging (GPI)[21] on the low-field-side midplane of the device. A poloidal section of Alcator C-Mod is shown in Fig. 1 with the outboard GPI views overlaid. GPI records fluctuations of the intensity of the light emitted by a locally introduced diagnostic neutral gas. The emissivity is mostly dominated by electron impact excitation, which makes the observed brightnesses sensitive to a combination of T_e and n_e. The light intensity has been shown[22] locally

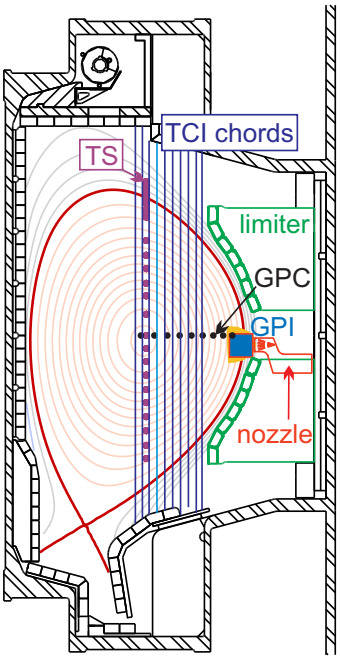

Figure 1. (color online) Configuration of the GPI viewing array (blue square) in a poloidal cross section view with a representative lower single null (LSN) magnetic equilibrium. The solid (red) D-shape curve represents the last closed flux surface (LCFS). The 10 vertical chords of the FTCI are overlaid in blue with the chord whose signals plotted in Fig. 4b in cyan. Measurement locations of Thomson scattering (solid purple circle) and ECE grating polychromators (GPC, black) are also displayed.

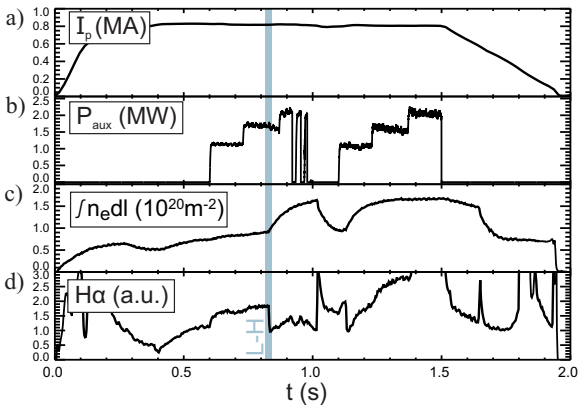

Figure 2. Plasma parameters from L-H transition experiment; a) Plasma current, b) auxiliary heating power, c) line integrated electron density from FTCI, d) deuterium Balmer α light, the sudden drop of which is the sign of the transition marked by the shaded blue area.

to behave as a power function of both: $I = An_e^{\alpha_n} T_e^{\alpha_T}$, so that for small fluctuations such as those observed in the plasma edge (typically $\delta n/n \lesssim 0.1$) yields a normalized fluctuation level of

$$\frac{\tilde{I}}{I} = \alpha_n \frac{\tilde{n}_e}{n_e} + \alpha_T \frac{\tilde{T}_e}{T_e}. \tag{8}$$

In the plasmas analyzed in this study $\alpha_T \approx 0.0 - 0.1$, while $\alpha_n \approx 0.5 - 0.6$, and consequently intensity fluctuations are considered to be density fluctuations.[23]

The diagnostic gas puff enters from a nozzle mounted in the limiter, 2.54 cm below the height of the magnetic axis. The GPI viewing array covers a two-dimensional area of considerable size at this location, extending both into the region of closed flux surfaces and into that of open field lines. The viewing area is 3.5cm(radial) × 3.9cm(vertical), with an in-focus spot size of 3.8mm for each of the 9×10 individual channels. All views are coupled to avalanche photodiodes (APD) sampled at 2MHz. In order to enhance the gas-puff-enhanced-to-background brightness ratio, we used He puffs into D plasmas, therefore the recorded intensities are band-pass filtered for the HeI ($3^3D \rightarrow 2^3P$), $\lambda = 587.6$nm line.

Velocimetry is based on a time-delay-estimation (TDE) method optimized for the fast 2D APD array, which has been demonstrated to yield sensible results[24]. Cross-correlations are calculated directly from the observed brightness fluctuations on neighboring channels, thus the time lag τ_m of the maximum correlation can yield reasonable time histories for the local phase velocity of emissive structures as simply $v_\theta = \Delta z/\tau_m$. Due to the high sensitivity and low noise of the diagnostic, a time resolution of $\sim 10\mu$s can be achieved, corresponding to a time lag estimated from samples as short as 20 frames. This 20 frame long sample pair is then moved forward frame by frame through the entire time history to provide velocimetry at every measurement point. Since this sample length introduces an effective Nyquist frequency of 50kHz in velocity measurements, turbulence velocities are low-pass filtered to this range in order to minimize noise. In addition slowly evolving quantities under the $\langle . \rangle$ averaging in the model are separated from the turbulence velocities by digitally high-pass filtering at 5kHz for $\tilde{v}$ and low-pass filtering at 3kHz for $\langle v \rangle$ so as to minimize overlap. While the particular cut-off values do not influence the main results of this paper, the choice was motivated by the lowest frequencies of geodesic-acoustic modes (GAM) found on Alcator C-Mod[24].

Sample results of this imaging based velocimetry are shown in Figure 3, exhibiting a rapid 1ms poloidal velocity burst at the L-H transition. The three plotted sample shots were run with very different operating conditions: the toroidal magnetic fields and plasma densities were different and the auxiliary heating power varied from none, i.e. a completely Ohmically heated plasma, to $P_{\mathrm{ICRF}} = 2.1$MW. The measured L-mode level poloidal velocities at a location $r - r_{\mathrm{LCFS}} \approx -6$mm inside the separatrix therefore showed a fair amount of variation. For better comparison the plotted curves are aligned in time by the L-H transition as determined from the drop of the D Balmer-α light, and the zero level is set to the average velocity in the L-mode phase before the transition.

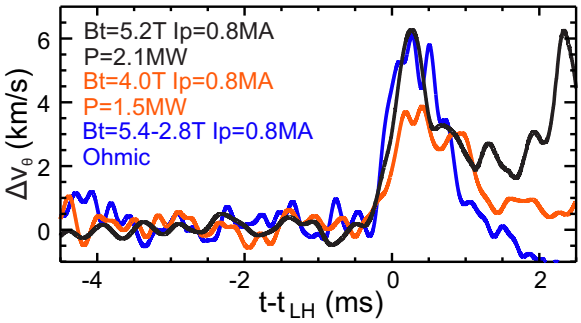

Figure 3. Zonal flow, i.e. the slow component of the time-delay-estimated poloidal velocity $\langle v_\theta \rangle$ at the transition at a radial location of $r - r_{LCFS} = -(5-8)$mm exhibiting the characteristic 1ms jolt in the EDD direction. Time bases of different plasma discharges are aligned by the drop of the D_α signal (t=0), and the average TDE poloidal velocity before transition is set as $v = 0$.

It is worth noting that although the poloidal velocity increments from L-mode seem to settle at widely different values *after* the transition, the poloidal velocity evolves quite similarly in the first 0.5ms of the transitions, which is the primary focus of this paper. Beyond this time temperature and density gradients start evolving, and in addition, measurements are less reliable, as the estimated errors grow to a value comparable to the velocity itself – both of which phenomena are discussed in more detail in the next section.

Owing to the fact that the edge fluctuations are expected to have a temperature gradient driven drift wave character, the slowly evolving component of the velocity spectrum from such a velocimetry algorithm is a combination of true flow and wave propagation. For consistent calculations in models using the fluid velocity, the GPI measured velocities must be corrected by the plasma frame wave propagation velocity $v_{d,e}$, i.e. the electron diamagnetic velocity to obtain the $\mathbf{E} \times \mathbf{B}$ speed $v_E = v_{GPI} - v_{d,e}$. For the bulk fluid velocity v_{fl}, this value must be further offset by the ion diamagnetic velocity $v_{d,i}$, such that $v_{fl} = v_{GPI} - v_{d,e} + v_{d,i}$ (Fig. 5). Thus the radial force balance is assumed to hold on the required time resolution in the zeroth order form

$$0 = E_r + v_{\theta,i} B_\phi - v_{\phi,i} B_\theta - \frac{1}{n_i Z_i e} \partial_r p_i, \tag{9}$$

i.e. neglecting the inertial terms with the assumption that flow acceleration is slow compared to force equilibration. This caveat holds for *all* studies of the L-H transition (or similarly dynamic processes) in which no direct E_r measurements are available, including those based on imaging or charge exchange spectroscopy. Therefore it can be instructive to confirm the validity of this assumption by directly measuring the local electric field. At the high edge densities and temperatures of Alcator C-Mod plasmas in RF heated L-H transitions Langmuir probe measurements are quite impossible. However, previous studies on other devices [4] *have* shown a good agreement between probe measurements and the E_r inferred from radial force balance, and thus the latter is taken here as well.

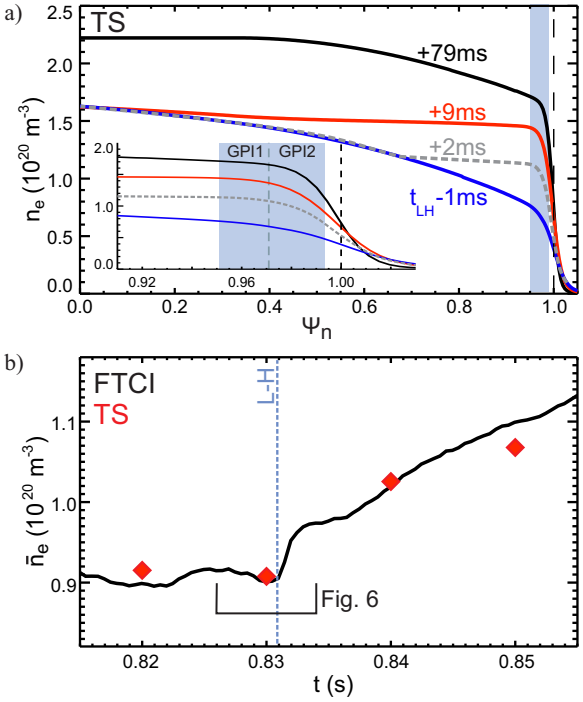

Figure 4. Evolution of electron density in the L-H transition; a) profiles fitted from combined Thomson scattering (TS) and electron cyclotron emission (ECE) measurements, b) line-integrated electron density as measured by fast two-color interferometer (solid line) and numerically integrated from the fits in part a) (red diamonds). Shaded blue areas indicate the location of GPI arrays providing the velocity and velocity-gradient measurements; the dashed blue line marks the time of the D_α-drop.

Both comparisons of the nonlinear transfer processes to the evolution of the edge gradients and the above calculation of the fluid velocity require the measurement of the edge gradients at a sub-millisecond time resolution. The relevant quantity in the momentum equation is the *ion* pressure gradient ∇p_i. However, the electron temperature has been known to be close to the ion temperature in the edge of Alcator C-Mod[25] $T_e \approx T_i$, and n_e is directly related to n_i by quasi-neutrality. The edge electron temperature is measured via a fast electron-cyclotron-emission (ECE) system with a radial resolution of $\sim$ 1cm, close to that of GPI, while the density profile is estimated with a combination of Thomson scattering (TS) and a recently upgraded fast two-color-interferometer (FTCI)[26] as follows. The TS system takes samples on a 10ms time base through the entire cross-section of the plasma, to which smooth radial profiles such as the ones in Figure 4a are fitted. For better orientation three time slices around the L-H transition are plotted in the figure in solid colors. The radial localization of the profiles is corrected by fitting the EFIT-mapped Thomson scattering T_e and n_e measurements and shifting them to match the expected values of T_e at the separatrix ($\psi_n = 1.0$), based on a two-point SOL-divertor power balance model. The evolution of the density profile shows the familiar image with a relaxed L-mode edge gradient just before the transition

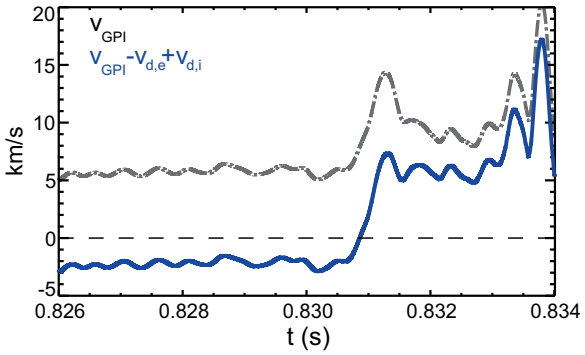

Figure 5. Estimated bulk poloidal velocity based on GPI velocimetry corrected with diamagnetic terms calculated from TS and ECE measurements.

($t - t_{\rm LH} = -1$ms), the intermediate state 9ms into the H-mode with the edge gradient already at the H-mode level and a relatively flat density profile which *just* reaches the L-mode core density at 1/3 the total flux. The core transport takes several tens of milliseconds to catch up to the new boundary condition, as illustrated by the curve 79ms after the transition, which has the same edge gradient as the early H-mode profile with the core gradients of a steady-state L-mode. Figure 4b shows the line-integrated electron density measurement of FTCI with four measurement points of the numerically integrated TS profiles overlaid, demonstrating an excellent match.

Furthermore, the high time resolution of the new FTCI system, reveals a reproducible, previously unobserved, $\sim$ 1ms phase of rapid growth (of $\sim$ 8%) at the beginning of the well-known (and much slower) linear increase in average density. Since in the evolution of the density profile the steep edge gradient is what forms first, we attribute this rapid growth in the FTCI signal to the formation of the pedestal. The local density and density gradient values are then inferred based on the following two assumptions: 1) that the gradient inside the pedestal region does not become positive (i.e. that core transport is always *fast enough* to form at least a flat density profile), and 2) that the core transport is *slow enough* to only reach a gradient inside the pedestal that is at most as steep as 9ms after the transition. While 1) is generally expected, 2) is clearly supported by evidence, since the L-mode core gradients take approximately 70ms to form. The profile with the dashed curve in Figure 4a is estimated with these two assumptions under the condition that the radial integral of the density match the FTCI measurement just after the rapid growth phase. Similar density profiles have been previously reported shortly after the formation of the H-mode pedestal.[27]

The velocity corrected by the diamagnetic terms calculated based on this density profile estimate is shown in Figure 5. While the absolute fluid velocity changes sign at the transition, the velocity increment in the first half millisecond of the transition is barely changed compared to the raw GPI measurement. In addition, the critical production term contains the radial gradient of the poloidal velocity, and due to the particular shape of the edge gradients, P calculated from $\partial_r v_{\rm fl}$ is well within the large error bars around P using $\partial_r v_{\rm GPI}$. Here we only note the fact that $v_{\rm fl}$ at $\sim$ 5mm inside

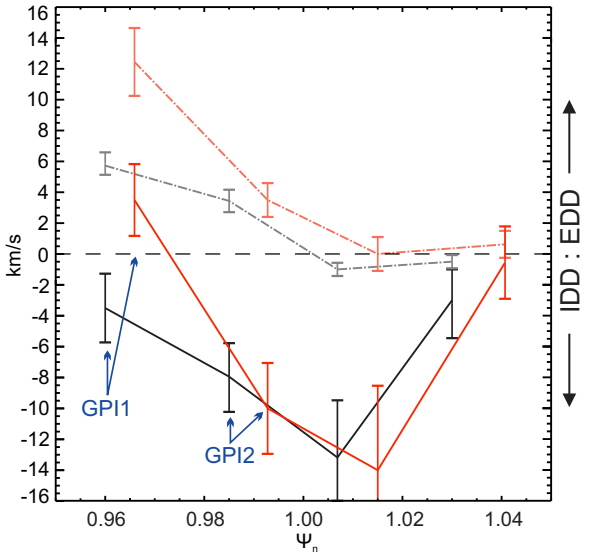

Figure 6. Radial profile of GPI measured poloidal velocities (dash-dot lines) before (black) and just at the transition (red) with fluid velocities (solid lines) estimated using ECE and FTCI. The sign convention: $V > 0$ is in the electron diamagnetic flow direction (EDD).

the last closed flux surface (LCFS) *stays large after the transition.* The specific radial locations marked as "GPI1" and "GPI2" over the shaded area in Fig. 4 at which detailed nonlinear analysis is performed is chosen on the basis of the radial profile of measured poloidal velocities, plotted in Fig. 6. The region between $\Psi_n = 0.96$ and $\Psi_n = 0.98$ exhibits the largest radial shear, thus it is the location of the largest nonlinear activity and forms the focus of our analysis. As is clear from the figure, the fluid velocities are estimated with a large error bar, due to the uncertainty in the edge gradients including both localization error and instrumental uncertainties. The red curves represent poloidal velocities averaged over the available poloidal range and over the 0.5ms velocity peak, while the black ones show a similar average 3.5ms before the designated transition time. The region where poloidal velocities show the most substantial change during the first millisecond of the transition is around 97% of the full magnetic flux, or $5-7$mm inside the LCFS, in both velocity estimates.

4. Results

One representative example of the results of this analysis is plotted in Figure 7 along with the key parameters of the L-H transition. The transition is achieved by an auxiliary heating power of $P_{\rm ICRF} = 1.75$MW under the most common conditions in Alcator C-Mod plasmas with $B_t = 5.2$T, $I_p = 0.8$MA, LSN geometry. The time of the transition is determined independently of the velocity measurements as the beginning of the sharp drop in the main chamber D_α signal, the most common indication of the onset of high global confinement. This instance is indicated as a dashed blue line in the figures as a point of orientation. As explained above, the quantities describing the turbulence–

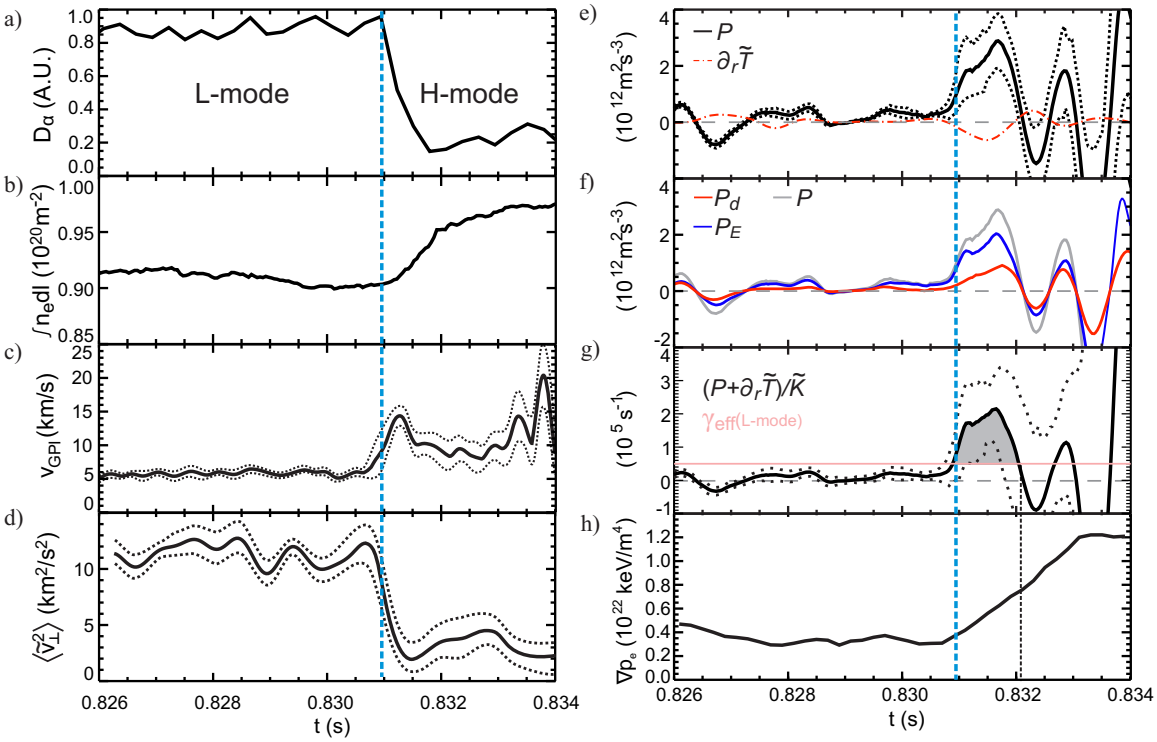

Figure 7. Evolution of key parameters in the L-H transition; a) main chamber D_α, b) line integrated n_e from FTCI, c) slow component of the GPI TDE ($\sim$ zonal flow) velocity, d) kinetic energy in turbulence $\langle \tilde{v}_\theta^2 \rangle$, e) kinetic energy transfer P from turbulence to shear flow, f) electric and diamagnetic components of P, and g) energy transfer rate. Dashed lines represent the extremes within the estimated experimental error. The pedestal pressure gradient is plotted in h), the second vertical dashed line marks the end of the production burst.

zonal-flow dynamics (Fig. 7c-f) are measured at a location $r - r_{\mathrm{LCFS}} = -6$mm inside the last closed flux surface. The results plotted in these graphs are reproduced very well in all of the studied L-H transitions.

The first growth in the low frequency, poloidally averaged GPI velocity is observed about $0.3 - 0.5$ms *before* the D_α drop, reaching its maximum acceleration just after the designated transition time (Fig. 7c). This burst is well correlated with the observed decrease in the kinetic energy stored in turbulence (Fig. 7d) which drops by about a factor of 5. The density perturbation component $\tilde{n}/n$ of the broadband edge turbulence has been previously shown in multiple experiments to suffer a similar reduction in the transition [21]. In fact, the sudden growth of the velocimetry error at the transition, as evidenced by Figs. 7c, is precisely due to this drop in the number of distinct density perturbations, as these are necessary for correct TDE measurements. Due to these errors of velocimetry just after the transition, comparing the amplitude reduction in the density- and velocity-perturbations is a useful cross-check method, which shows that the initial loss of turbulent *density* fluctuation power ($t = 0.8305\mathrm{s} - 0.8315\mathrm{s}$) is indeed a factor of ≈ 10, close to that observed in Fig. 7d as $\tilde{K}_{\mathrm{L-mode}}/\tilde{K}_{\mathrm{min}} = 3 - 14$.

Consistent with the expectation from probe measurements[10] on other devices and the Kim–Diamond predator–prey model[18, 9], the production term $P = \langle \tilde{v}_r \tilde{v}_\theta \rangle \partial_r \langle v_\theta \rangle$ exhibits a rapidly growing peak in time during these changes (Fig. 7e). Although the turbulence spreading term, plotted in the same panel on the same scale, is in the opposite direction, its magnitude is at most 1/4 of P and is not sufficient to offset it. Since neither the local temperature gradient nor the density gradient is changing until at least 1ms after the first spike in P according to TS and ECE measurements, and even the total pressure gradient across the entire pedestal region grows by at most roughly a factor of two; the effective turbulence growth rate γ_{eff} is expected to be unchanged through this first evolution of kinetic energy transfer. Thus, P is expected to dominate the rate of change in the turbulent kinetic energy during this early period.

In order to see whether the growth in P is responsible for the reduction of turbulence in (7), γ_{eff} is estimated from the L-mode phase as follows. A stationary period of the L-mode phase can be suitably chosen, in which the turbulent kinetic energy $\tilde{K}$ is invariant, such that the effective turbulent energy input $\gamma_{\text{eff}}\tilde{K}$ is balanced by the local losses $P + \partial_r \tilde{T}$, leading to the estimate

$$\gamma_{\text{eff}}|_L = \left[\frac{P + \partial_r \tilde{T}}{\tilde{K}} \right]_{\text{L-mode}} \tag{10}$$

Our analysis of the stationary L-mode data obtained in the 20ms period before the L-H transition yields $P \simeq 6.5 \pm 5.0 \times 10^{11} \text{m}^2\text{s}^{-3}$ in L-mode, with a negligible contribution from $\partial_r \tilde{T}$ at this location. With the observed approximate value of $\tilde{K} = 12 \pm 2 \text{km}^2\text{s}^{-2}$, we estimate $\gamma_{\text{eff}}|_L = 0.6 \pm 0.5 \times 10^5 \text{s}^{-1}$. Next turning our attention to the period of the L-H transition, we observe in Fig. 7g that the rate $(P + \partial_r \tilde{T})/\tilde{K}$ exhibits a rapid (~ 0.5ms) increase and reaches a peak value of $\sim 2 \times 10^5 \text{s}^{-1}$ during this transient. Thus for this period we see that $(P + \partial_r \tilde{T})/\tilde{K}\gamma_{\text{eff}} \approx 3$, satisfying condition (7). Note that due to the estimation of $\gamma_{\text{eff}}|_L$ from the L-mode state, the dimensionless growth-loss ratio parameter is inherently close to 1, and therefore it is understood that the ratio in condition (7) must be *significantly* bigger than one. Given the short time span of the excursion in $(P + \partial_r \tilde{T})/\tilde{K}\gamma_{\text{eff}}$ we are lead to ask the question whether this interaction indeed transfers enough energy during this period to explain the observed reduction of the turbulence amplitude and thus be held responsible for the phase transition. For this quantitative consistency check, we turn once again to Eq. 4. Although $\tilde{K}$ and $P + \partial_r \tilde{T}$ are clearly time-dependent during the L-H transition, γ_{eff}, with its theoretical dependence primarily on ∇T, ∇n, is not expected to vary until the edge gradients are significantly altered. Then the integral of the equation can be written as

$$R_K \equiv \ln \frac{\tilde{K}_{\text{L}}}{\tilde{K}_{\text{min}}} = \int_{t_0}^{t_m} \left[\frac{P + \partial_r \tilde{T}}{\tilde{K}} - \gamma_{\text{eff}} \right] dt \equiv R_P, \tag{11}$$

where $\tilde{K}_{\text{min}} = \tilde{K}(t_m)$ is the minimal amount of turbulence in the transition, which is reached at time t_m, while t_0 denotes a time before the transition when the average level of turbulence is equal to the L-mode value preceding the transition. Equation (11)

also introduces a shorthand notation for the dimensionless measures describing how the observed reduction in turbulence R_K compares to the total amount of power transferred into the zonal flow R_P. The shaded area in Fig. 7g illustrates the estimation of the latter via the above integral. The values from the experiment depicted in the figures are $R_K \approx 2.3$, $R_P = 210 \pm 160$, bringing the estimated total of the transferred kinetic energy to a much *larger* value than the observed drop in turbulence power. Given the uncertainties associated with the measurement of small perturbations in both the density and the velocity component of the turbulence, as well as the poloidally localized nature of the edge turbulence which is likely to lead to an overestimate of R_P, these results do not contradict the conclusion that *the lossless energy conversion mechanism from the broadband turbulence to a fluctuation driven flow is sufficiently strong to explain the collapse of turbulence* in the L-H transition.

For the complete consistency of the argument, the balance of the low frequency fluid flow evolution was also examined. The terms with a time history which depend only on the low-frequency flow component $\langle v_\theta \rangle$ are the zonal kinetic energy growth $\bar{K}$ and the collisional damping $\nu_{\rm LF}\bar{K}$. The low frequency damping rate in the expression is estimated similarly to the effective growth rate from the time average component of (5) as

$$\nu_{\rm LF}|_L = \left[\frac{\partial_r \langle \tilde{v}_r \tilde{v}_\theta \rangle}{\langle v_\theta \rangle} \right]_{\rm L-mode}. \tag{12}$$

The resulting value $\nu_{\rm LF}|_L = 4 \pm 3 \times 10^3 {\rm s}^{-1}$ is approximately an order of magnitude smaller than the neoclassical damping rate of geodesic acoustic modes (GAM)[28] recently found in Alcator C-Mod plasmas [24], in line with theoretical expectations. With this estimate, the low-frequency terms of the kinetic energy evolution $(\partial_t \bar{K} + \nu_{\rm LF}\bar{K})$ are plotted in Figure 8 alongside the Reynolds work $P - \partial_r \bar{T} = \langle v_\theta \rangle \partial_r \langle \tilde{v}_r \tilde{v}_\theta \rangle$, demonstrating a striking degree of similarity, indicating that the Reynolds work dominates the transition. The production term without the contribution from $\partial_r \bar{T}$ is shown overlaid, and shows a very poor level of correlation to the other two quantities, demonstrating the importance of considering the radially extended character of the zonal flow drive, i.e. a 1-spatial dimension model over simpler 0D models[10, 11, 20].

Finally, the timing of the edge radial electric field and pressure gradient evolution is examined in some detail. While the direct GPI measured poloidal velocity consistently shows a short pulse during the transition, as demonstrated in Fig. 3, the velocity corrected for the diamagnetic flow in Fig. 5 exhibits a character more familiar from previous transition studies[29] with a rapid shift in the EDD direction, without a relaxation later in the H-mode phase. This suggests that the recovery phase in the GPI velocities is due to the relatively slow growth of the pressure profile, which apparently occurs during the following $\sim$ 3ms of the H-mode. Using our profile evolution measurements, the $\mathbf{E} \times \mathbf{B}$ and diamagnetic components can be similarly separated in the production term as $P = \langle \tilde{v}_r \tilde{v}_\theta \rangle \partial_r (v_E + v_{d,i}) = P_E + P_d$, where v_E is the local $\mathbf{E} \times \mathbf{B}$ velocity, $v_{d,i}$ is the diamagnetic ion flow, $P_E = \langle \tilde{v}_r \tilde{v}_\theta \rangle \partial_r v_E$, and $P_d = \langle \tilde{v}_r \tilde{v}_\theta \rangle \partial_r v_{d,i}$. Figure 7f plots both components against time at the transition, demonstrating once

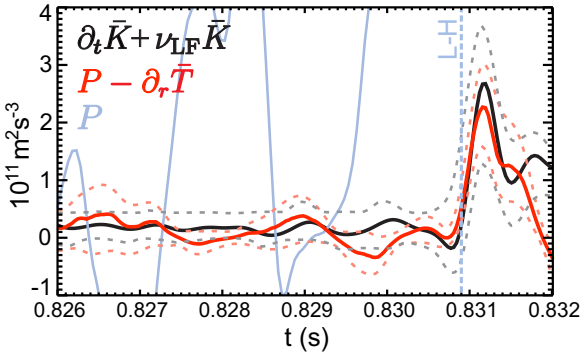

Figure 8. (color online) Evolution of the Reynolds work (solid red) and the sum of the measured rate of kinetic energy change $\partial_t \bar{K}$ and damping $\nu_{\rm LF} \bar{K}$ (black) around the time of the L-H transition. The pale blue curve represents the production component P of the Reynolds work $P - \partial_r \bar{T}$ for comparison.

again that the original rapid growth in the production term is due to energy transfer into the electric component of the flow. All the above give further justification for not *explicitly* including the more slowly evolving gradient-driven, diamagnetic terms in the kinetic energy transfer analysis.

5. Discussion

In addition to being among the first few imaging based experiments corroborating recent probe measurements from the edge of tokamak plasmas[10], the results presented in the previous sections also include the first quantitative comparison between the reduction of edge turbulence and the energy transferred into zonal flows in the same radial location. As a further advantage of imaging, the analysis that was demonstrated in Fig. 7 became much more accessible than probe measurements inside the LCFS, allowing a large number of experiments to be performed, the results of which are summarized in Figure 9. The evolution of the key transfer quantities was very similar from one shot to the next. In the quantitative analysis, the normalized amount of kinetic energy converted was consistently quite substantially larger than the observed reduction in turbulence power, albeit with large error bars on both quantities. Due to the difficulty of setting a lower bound on very small turbulent fluctuations of both density and velocity, it is possible that the full turbulence reduction ratio is greater than observed on any diagnostic. In addition, one must of course realize that the poloidal averages applied in the analysis are restricted to the extent of the imaging arrays, and consequently larger areas need to be sampled if one expects to find more exact matches. Nevertheless, this result strongly suggests that the discussed *lossless nonlinear energy transfer from the broadband turbulence to zonal flows via the action of the Reynolds stress is sufficient to explain the initial reduction of turbulence power*, and is thus a key player in mediating the L-H transition.

Furthermore, it has been shown that the flow drive afforded by the Reynolds work

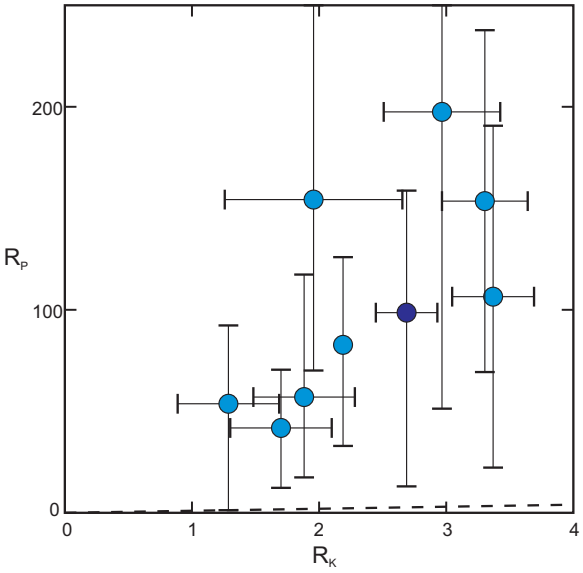

Figure 9. Reduction of turbulence vs normalized total energy transfer across shots. The dashed line represents $R_K = R_P$, demonstrating that R_P is commonly observed to be much larger than the reduction in turbulence. The shot studied in detail is marked dark.

done by turbulent fluctuations is sufficient to explain the local growth of the fluid flow. This result also confirms the identity of the shear flow as a zonal flow in the sense that it is "the turbulence driven component of the $\mathbf{E} \times \mathbf{B}$ shear flow."

In order to enter a fully developed H-mode, two criteria must be satisfied: 1) first the edge turbulence, which dominates cross-field transport must be reduced, then 2) turbulence must be kept at a suppressed level relative to L-mode. Our results show that the condition expressed in (7) is a reliable indicator of the onset of the first turbulence quenching. The single predator single prey model without any evolution of the pressure-gradient-driven $\mathbf{E} \times \mathbf{B}$ shear flow was shown in Refs. [18, 9] to produce limit cycle oscillations. The drift wave turbulence (the prey population) is depleted leading to an extinction of the zonal flow (predator), which in turn leads to the recovery of turbulence and hence the repetition of the cycle. These oscillations have in fact been experimentally demonstrated close to the H-mode threshold.[30] The second step to a sustained H-mode, i.e. a permanent suppression of turbulence, is therefore a growth of the edge pressure gradient (a second predator) *during* the phase when turbulence is reduced by the zonal flow. It is therefore very instructive to examine the evolution of the edge pressure gradient during the period of significant energy transfer. The methods outlined in the section explaining the estimation of $v_{d,i}$ fully equip us to perform this analysis, and the result is plotted in Figure 7h.

In the 1ms time period with a large positive production P, the edge pressure gradient grows approximately 100%. Since the edge pressure gradient slowly fluctuates during the low confinement regime with an amplitude of approximately 30%, one can empirically conclude that the critical amount of pressure gradient growth sufficient for

turbulence suppression is in the $30\% - 100\%$ range. This result is also in good agreement with the typical reported limit-cycle period of ~ 0.3ms[30] during which the pressure gradient would only increase by 30%, quoted above as a typical L-mode level edge gradient variation.

The above results unambiguously establish the time sequence of the L-H transition as: *first* the peaking of the normalized Reynolds power, *then* the collapse of the turbulence, and *finally* the rise of the diamagnetic electric field shear. Since the growth of the pressure gradient in the region exhibiting turbulence suppression is directly related to the heat flux entering this region from the plasma core, this result provides a key element in connecting the microscopic physics to the L-H power threshold in large scale operating parameters such as heating power and plasma density.

Acknowledgments

The authors would like to thank the Alcator C-Mod team of students, scientists, engineers and technical staff for making the experiments possible. This work is supported by U.S. Department of Energy Cooperative Agreement No. DE-FC02-99ER54512

References

[1] I. H. Hutchinson, R. Boivin, F. Bombarda, P. Bonoli, S. Fairfax, C. Fiore, J Goetz, S. Golovato, R. Granetz, M. Greenwald, et al. *Phys. Plasmas*, 1:1511, 1994.

[2] F. Wagner, G. Becker, K. Behringer, D. Campbell, A. Eberhagen, W. Engelhardt, G. Fussmann, O. Gehre, J. Gernhardt, G. v. Gierke, et al. *Phys. Rev. Lett.*, 49:1408, 1982.

[3] R. J. Groebner, K. H. Burrell, and R. P. Seraydarian. *Phys. Rev. Lett.*, 64:3015, 1990.

[4] R. A. Moyer, K. H. Burrell, T. N. Carlstrom, S. Coda, R. W. Conn, E. J. Doyle, P. Gohil, R. J. Groebner, J. Kim, R. Lehmer, et al. *Phys. Plasmas*, 2:2397, 1995.

[5] F. Wagner. *Plasma Phys. Control. Fusion*, 49:B1B33, 2007.

[6] P. H. Diamond, S. Itoh, K. Itoh, and T. S. Hahm. *Plasma Phys. Control. Fusion*, 47:R35, 2005.

[7] A. Fujisawa. *Nucl. Fusion*, 49:013001, 2009.

[8] A. D. Liu, T. Lan, C. X. Yu, H. L. Zhao, L. W. Yan, W. Y. Hong, J. Q. Dong, K. J. Zhao, J. Qian, J. Cheng, et al. *Phys. Rev. Lett.*, 103:095002, 2009.

[9] K. Miki, P. H. Diamond, Ö. D. Gürcan, G. R. Tynan, T. Estrada, L. Schmitz, and G. S. Xu. *Phys. Plasmas*, 19:092306, 2012.

[10] P. Manz, G. S. Xu, B. N. Wan, H. Q. Wang, H. Y. Guo, I. Cziegler, N. Fedorczak, C. Holland, S. H. Müller, S. C. Thakur, M. Xu, K. Miki, P. H. Diamond, and G. R. Tynan. *Phys. Plasmas*, 19:072311, 2012.

[11] G. R. Tynan, M. Xu, P. H. Diamond, J. A. Boedo, I. Cziegler, N. Fedorczak, P. Manz, K. Miki, S. Thakur, L. Schmitz, et al. *Nucl. Fusion*, 53:073053, 2013.

[12] C. P. Ritz and E. J. Powers. *Physica D*, 20:320, 1986.

[13] C. P. Ritz, E. J. Powers, and R. D. Bengtson. *Phys. Fluids B*, 1:153, 1989.

[14] Y. Kim, R. D. Durst, R. J. Fonck, A. Ware, and P. W. Terry. *Phys. Plasmas*, 3:11, 1996.

[15] C. Holland, G. R. Tynan, R. J. Fonck, G. R. McKee, J. Candy, and R. E. Waltz. *Phys. Plasmas*, 14:056112, 2007.

[16] M. Xu, G. R. Tynan, C. Holland, Z. Yan, S. H. Muller, and J. H. Yu. *Phys. Plasmas*, 16:042312, 2009.

[17] S. B. Pope. *Turbulent Flows*. Cambridge University Press, Cambridge, UK, 2000.
[18] E. Kim and P. H. Diamond. *Phys. Rev. Lett.*, 90:185006, 2003.
[19] C. Hidalgo, C. Silva, M. A. Pedrosa, E. Sanchez, H. Fernandez, and C. Varandas. *Phys. Rev. Lett.*, 83:2203, 1999.
[20] P. Manz, M. Xu, N. Fedorczak, S. C. Thakur, and G. R. Tynan. *Phys. Plasmas*, 19:012309, 2012.
[21] I. Cziegler, J. L. Terry, J. W. Hughes, and B. LaBombard. *Phys. Plasmas*, 17:056120, 2010.
[22] D. P. Stotler. *J. Nucl. Mat.*, 313-316:1066, 2003.
[23] I. Cziegler. *Turbulence and Transport Phenomena in Edge and Scrape-Off-Layer Plasmas*. PhD thesis, MIT Plasma Science and Fusion Center, 2011.
[24] I. Cziegler, P. H. Diamond, N. Fedorczak, P. Manz, G. R. Tynan, M. Xu, R. M. Churchill, A. E. Hubbard, B. Lipschultz, J. M. Sierchio, et al. *Phys. Plasmas*, 20:055904, 2013.
[25] R. M. McDermott, B. Lipschultz, J. W. Hughes, P. J. Catto, A. E. Hubbard, I. H. Hutchinson, R. S. Granetz, M. Greenwald, B. LaBombard, K. Marr, M. L. Reinke, J. E. Rice, D. Whyte, and Alcator C-Mod Team. *Phys. Plasmas*, 16:056103, 2009.
[26] C. P. Kasten, J. H. Irby, R. Murray, A. E. White, and D. C. Pace. *Rev. Sci. Instrum.*, 83:10E301, 2012.
[27] M. E. Manso. *Plasma Phys. Control. Fusion*, 35:B141, 1993.
[28] S. V. Novakovskii, C. S. Liu, R. Z. Sagdeev, and M. N. Rosenbluth. *Phys. Plasmas*, 4:12, 1997.
[29] E. J. Doyle et al. In *Plasma Physics and Controlled Nuclear Fusion Research (Proc. 14th Int. Conf. Wurzburg, 1992)*, volume 1, page 235, 1993.
[30] L. Schmitz, L. Zeng, T. L. Rhodes, J. C. Hillesheim, E. J. Doyle, R. J. Groebner, W. A. Peebles, K. H. Burrell, and G. Wang. *Phys. Rev. Lett.*, 108:155002, 2012.